Reprinted from SPIE Vol. 925—Ocean Optics IX

Concurrent particle and optical measurements in western Sargasso Sea

Alan D. Weidemann, Dennis M. Lavoie, and Rudolph Hollman

Naval Ocean Research and Development Activity
John C. Stennis Space Center, Mississippi, 35929-5004

Michael R. Wilcox

Planning Systems Inc., 115 Christian Lane, Slidell, Louisiana, 70458

ABSTRACT

Concurrent water samples and optical profiles were taken at twelve stations in the Western Sargasso Sea, at approximately 34°N and 70°W (Biowatt Mooring) during August 1987. Optical measurements included up- and downwelling scalar and vector irradiance. In situ relative fluorescence and beam transmission at 660 nm revealed a particle layer the center of which varied between 70 and 110 m and had a breadth of 20 to 40 m. Water samples were collected within the particle layer and near surface and analyzed for particle characterization and volume absorption.

Absorption coefficients for the near surface and particle layer were calculated using three techniques. Two techniques employed measurements of apparent optical properties. One method utilized scalar and vector irradiances and calculated absorption as the product of the average cosine and the diffuse attenuation coefficient for net irradiance at wavelengths of 441 and 520 nm. The second method used inversion of the irradiance quartet (up- and downwelling vector and scalar irradiances) and also calculation of absorption from only up-and downwelling vector irradiances. In the third method, absorption coefficients were calculated as the sum of particulate, dissolved substances, and molecular water absorption. Some large discrepancies were found between absorption from apparent properties and those calculated from the component sum. Possible sources of error include overestimation of dissolved substance or particulate absorption, inaccurate pure water absorption, and influence of internal radiance sources, such as Raman scattering, on apparent optical properties. (Reprints, 1&2)

Particles were characterized by three different techniques: relative particle concentration by in situ transmissometry at 660 nm; particle frequency and volume distributions by resistive pulse technique ("Coulter counts"); and particle frequency and size/shape distribution vs. elemental composition by SAX (Scanning electron microscopy with Automated image analysis and X-ray spectroscopy). Total particle number decreased with depth and was largely due to decreasing concentration of organic particles. There was a small size increase in siliceous particles near depths of the fluorescence maxima. In contrast, backscatter values derived from apparent optical properties increased by nearly two-fold from the surface to depth of maximum fluorescence.

1. INTRODUCTION

Absorption and scattering are fundamental processes governing light attenuation in natural waters. Preisendorfer[1] has distinquished between inherent optical properties, such as the volume absorption and scattering coefficients which are functions of the medium and are independent of the directional nature of the light field, from apparent optical properties, such as the diffuse attenuation coefficient (K) and irradiances which are dependent on the light field. There are no accepted methods to independently measure absorption and scattering coefficients in situ; however, absorption and scattering can be estimated from laboratory measurements of discrete water samples or they can be derived through inversion of radiative transfer models which use apparent optical properties such as measured up- and downwelling irradiances. A goal of the Naval Ocean Research and Development Activity (NORDA) optical oceanography program is deriving inherent optical properties for various ocean environments, then checking the volume or "bulk" optical properties for internal consistency using Monte-Carlo simulation.

Even though various techniques to estimate the inherent optical properties have existed for some time, few investigators have attempted to compare laboratory measurements of bulk properties with inherent properties derived from theoretical models that use apparent properties as inputs. We present optical and particle data from which the absorption coefficient is estimated for blue and green light from three methods: laboratory measurement of discrete water samples, inversion of in situ irradiance measurements, and solution of the radiative transfer equation for net irradiance.

2. THEORY

2.1. Absorption via Stavn

Stavn[2] expanded on the classic work of Gershun and Schellenberger[3] to derive what he termed the three-parameter model for a light field. In his work the absorption coefficient for a depth interval is calculable from measurements of up- (E_u) and downwelling (E_d) vector and scalar (E_o) irradiances. Whereas other treatments have largely ignored changes in the average cosine (mean light path) that may occur over a depth interval, Stavn showed that this may lead to an overestimate in absorption. The absorption coefficient ($\underline{a}$) for a depth interval z_1 to z_2 is given for the interval by

$$a = [\ln E_z(z_2) - \ln E_z(z_1)]/\Delta Z \quad (1)$$

where $E_z = E_d - E_u$ = net irradiance

$$\Delta Z = \int_0^{z_2} dz/u - \int_0^{z_1} dz/u$$

u = average cosine given by (E_z/E_o)

The mean light path (Z above) retains the information regarding variation in the average cosine or changes in light path occurring within the depth interval over which absorption is being calculated. Equation (1) can be written as

$$a = u\, K_e \quad (2)$$

from the definition of the diffuse attenuation coefficient for net irradiance (K_e) and with u averaged over the same space and time interval from which K_e is calculated. The Stavn three-parameter model[3,4] is limited in that, while the absorption coefficient can be extracted, the scattering coefficient cannot.

2.2. Absorption via Preisendorfer/Mobley

By contrast, both absorption and backscattering coefficients can be obtained from inversion of the irradiance quartet[5] (up- and downwelling scalar and vector irradiances). Preisendorfer and Mobley[5] have suggested that, for most natural waters the upwelling (E_u/E_{ou}) and downwelling (E_d/E_{od}) average cosines are approximately constant with values of 1/2.54 and 1/1.33, so that the volume absorption $\underline{a}$ and volume backscatter b_b can be calculated simply from the up- and downwelling vector irradiances.

2.3. Absorption by components

Because absorption is an inherent property, it can be partitioned into its components so that the contribution from water a_w, particulates a_p, and dissolved substances a_y can be evaluated.[6,7]. Thus,

$$a = a_w + a_y + a_p \quad (3)$$

Inasmuch as K, the diffuse attenuation coefficient is an apparent optical property, the same type of breakdown into components does not apply[8].

The presence of internal radiance sources such as, particulate and dissolved material fluorescence, Raman scattering, or bioluminescence can significantly influence the values of absorption derived from the apparent optical properties, but in general they will have a small impact on the absorption calculated independently from the components. Therefore, a comparison of absorption values from components with those derived from apparent optical properties has potential for quantifying the combined effects of bioluminescence, fluorescence, and Raman scattering.

3. METHODS

3.1. Sampling area and mode

Optical and particle data were collected at one station along the north wall of the Gulf Stream and at twelve stations in the general vicinity of the Biowatt mooring at ~34° N and 72° W. We report here preliminary results for two stations near the Biowatt mooring, Stations 8 and 11. Deployment at Station 8 (21 August) was a typical vertical cast whereas Station 11 (22 August) consisted of 3-5 minute time series at depths of 10, 30, 65, 75, and 100 m.

3.2. Optical and hydrographic measurements

Optical data and water samples were collected with a Particle/Optical Sampling System (POSSY), consisting of in situ instrumentation attached to a General Oceanics (Miami, Fl.) rosette with eight liter Niskin water samplers. The optical suite consisted of a Biospherical Instruments, Inc. (San Diego, Ca.) MER-1048 spectroradiometer which measured down- (13 wavelengths) and upwelling (8 wavelengths) vector irradiance, upwelling radiance (8 wavelengths), and up- and downwelling scalar irradiance (4 wavelengths each). Due to the loss of a downwelling scalar sensor, the complete optical quartet was only available for 441, 488, and 520 nm.

Beam transmission was measured with a 25 cm path length Sea Tech, Inc. (Corvallis, Or.) transmissometer, and relative fluorescence was measured with a Seamartec, Inc. (Seattle, Wa.) in situ fluorometer. Outputs from both instruments were multiplexed into the FSK signal sent to the surface by the MER. Temperature and conductivity were measured using Sea-Bird Electronics Inc. (Belleview, Wa.) modular sensors whose outputs were also multiplexed into the FSK output.

Water samples were collected on upcasts or during time series for particle analysis (elemental composition, size, concentration, volume), and dissolved material and particulate absorption spectra. Dissolved absorption was measured from 320 to 760 nm on the filtrate passing through a 0.2um nucleopore filter using a Kontron Uvikon Model 860 (Everett, Ma.) spectrophotometer. Because dissolved substance absorption was so small, the natural log of absorbances were plotted against wavelength from 320 to 420 nm, and the exponential rate of decrease was calculated. This was then used to extrapolate dissolved absorption at 441 and 520 nm. Particulate absorption[9] was determined using GF/C filters following procedures put forth by Mitchell and Kiefer[9]. Particle concentrations and size distributions were measured by two techniques. The first was the standard "Coulter" or resistive pulse technique using a Particle Data Inc. (Elmhurst, Il.) Model 80-XY counter. The second was an automated microscopy technique that uses a scanning electron microscope, image analyzer, and X-ray spectrometer combined with heavy metal staining[10] to yield additional information on particle composition.

3.3. Irradiance data processing

The high temporal resolution (5 Hz) of the optical data allowed for the resolving of sources of contamination. A notch filter was applied to the raw data to remove irradiance fluctuations that were linked to ship motion and tilt-roll of the instrument package. A technique similar to that used by Smith and Baker[11] was employed to smooth out effects of wavefocusing on calculated values of K_e. Because its variance was much smaller than that of K_e, the average cosine was calculated from the arthimetic mean over the same interval as for K. To account for temporal changes in incident light, irradiances were normalized to deck cell measurements.

For the Preisendorfer-Mobley inverse model, irradiance data was binned within $\pm$0.1 m of each integer depth for profile Station 8. For Station 11, irradiances at each integer depth were calculated from the time averages at each of the five depths, normalized to the appropriate deck cell (to remove atmospheric variability). These values were then used to calculate the average irradiances at intervening depths that were used as input into the Preisendorfer-Mobley model. The application of splining techniques were unsatisfactory due to the limited number of data points.

4. RESULTS AND DISCUSSION

4.1. Temperature, fluorometry, transmissometry

Hydrographically, the mixed layer was isothermic at ~23.2 C from the surface to 35 m, from which depth the temperature declined at a steady and slow rate of 0.06 C m^{-1} to at least 200 m. The beam transmissometry profile for Station 11 varied +0.2% about 88.3 between the surface and 200 m. Relative fluorescence was very low, virtually at zero for most of the water column except between 150 to 165 m and between 65 and 110 m (SEM examination revealed the presence of chain-forming diatoms only at the 75 m sample depth). In each of these two layers, relative fluorescence rose only to about 5% on the most sensitive scale. The beam transmission did not show any structure at the more shallow fluorescence peak, but it did exhibit a small decrease at the deeper maximum. At Station 8, the in situ fluorescence layer was between 80 and 120 m peaking at ~100 m. At either station, extracted chlorophyll were low at all depths rising to only 0.1 ug l^{-1} in the maximum.

4.2. Absorption coefficients

Absorption measurements are calculated for two wavelengths, 441 and 520 nm, to yield information on the spectral dependency of bulk absorption. The absorption by molecular water a_w for 441 nm has been reported to be 0.014 m^{-1} versus 0.048 m^{-1} for 520 nm[12].

Table 1. Bulk absorption of water, dissolved substances, and particulates (m^{-1})

Station 8 441 nm depth (m)	Absorption (m^{-1}) a_w	a_y	a_p	$\underline{a}$	uK_e	a'	a"
10	0.014	0.011	0.013	0.038	0.012	0.014	0.014
34	0.014	0.025	0.013	0.052	0.017	0.018	0.018
100	0.014	0.029	0.039	0.082	0.053	0.055	0.051
Station 8 520 nm depth (m)							
10	0.048	0.003	0.004	0.055	0.042	0.047	0.040
34	0.048	0.006	0.003	0.057	0.039	0.041	0.035
100	0.048	0.007	0.008	0.063	0.041	0.043	0.052
Station 11 441 nm depth (m)							
11	0.014	0.016	0.012	0.042	0.014	0.016	
31	0.014	0.009	0.014	0.037	0.018	0.016	
62	0.014	0.011	0.020	0.045	0.029	0.029	
80	0.014	0.015	0.036	0.065	0.039	0.044	
107	0.014	0.009	0.015	0.038	0.038	0.047	
Station 11 520 nm depth (m)							
11	0.048	0.004	0.005	0.057	0.041	0.043	
31	0.048	0.002	0.004	0.054	0.040	0.040	
62	0.048	0.002	0.005	0.055	0.042	0.042	
80	0.048	0.003	0.011	0.062	0.044	0.042	
107	0.048	0.002	0.004	0.054	0.044	0.043	

$\underline{a} = a_w + a_y + a_p$
a' = absorption derived from Preisendorfer/Mobley using calculated distribution factors.
a" = absorption derived from Preisendorfer/Mobley assuming distribution factors of 2.67 and 1.33 for up- and downwelling radiance respectively.
uK_e = absorption calculated using Stavn's three-parameter method.

4.3. Absorption by dissolved substances

Stations 8 and 11 differ markedly in the absorption attributed to dissolved substances (Table 1); however, the shape of the absorption spectra were quite similar. The slope of the log-linear relationship between ln of absorption and wavelength over the interval 320-420 nm was 0.015-0.020 with a mean of 0.017 at both stations. This range for the rate of extinction is the same as that found by others[13,14]. Using absorption at 380 nm as a reference ($a_y(380)$), station 8 had absorption values that ranged from 0.03 to 0.08 m^{-1}, and station 11 had values less than 0.05 m^{-1}. The $a_y(380)$ at other stations ranged from near detection limits to ~0.05 m^{-1}. These values are generally in the range found by other studies for oligotrophic oceans[14] (they range from near zero to 0.05 m^{-1} with a mean of 0.03 m^{-1}).

The absorption ascribed to dissolved substances showed a strong relationship to particle absorption and in situ fluorescence. Presumably this represents a non-conservative fraction that is a decay product of phytoplankton[14]. At both stations, a_y increased by nearly a factor of 2 near depths of higher relative fluorescence.

4.4. Particulate absorption

The magnitude of particulate absorption was the same at Stations 8 and 11. Absorption ascribed to particulates was approximately 0.013 m^{-1} near the surface and increased nearly three-fold in samples collected at or near the fluorescence maximum.

4.5. Bulk absorption coefficients

Station 8

Station 8 was a vertical profile, and exhibited high a_y. Irradiance data were in one m increments. There was excellent agreement between absorption coefficients derived from the three-parameter model of Stavn and the Preisendorfer/Mobley inverse model, which assumed distribution factors (the reciprocal of average cosines) of 1.33 and 2.67 for down- and upwelling light respectively (Figure 1). At 441 nm the absorption coefficients derived from the models using apparent optical properties rise from near that of "pure water" ($0.014\ m^{-1}$) at the surface to $0.047\text{-}0.050\ m^{-1}$ at the fluorescence maxima. In clear waters, where multiple scattering is negligible, it was anticipated that the Stavn and Preisendorfer/Mobley models would yield similar results, because both are highly dependent on the derivative of downwelling vector irradiance. Including the scalar irradiances and calculating the distribution factors (or average cosines) rather than using the constants of 2.67 and 1.33 did little to change the absorption estimate for 441 nm (see Figure 2) in the Preisendorfer/Mobley model.

The results at 520 nm were similar in that the Stavn and Preisendorfer/Mobley models yielded similar absorption estimates; however, this was only true if the distribution factors were calculated from the irradiance quartet instead of using 1.33 and 2.67. The Preisendorfer/Mobley estimates of absorption (using the calculated distribution factors) rose from ~0.040 above 50 m to >0.045 below 50 m; whereas the absorption coefficient from the three-parameter model was ~0.046-0.050 m^{-1} from 10 to 70 m then declined to 0.040 by 100 m. if 1.33 and 2.67 were used for the distribution factors, absorption values ranged from 0.03 to 0.08 m^{-1} and were highly variable with depth.

In contrast to the general agreement between the estimates of absorption derived from the models, there is a large disparity between the model-derived values and those measured spectrophotometrically (the sum of the components). the sum of the components at 441 nm is two-fold higher than the absorption values derived from the models for the upper 30 m, although agreement improves with increasing depth. also, there are many values for 520 nm absorption which fall below $0.048\ m^{-1}$, the absorption ascribed to molecular water, that can be attributed to raman scattering[15].

Station 11

Station 11 consisted of five time series and exhibited low a_y values. Irradiance data were interpolated among the five depths. The time series samples are spaced at depth increments that are too large to properly estimate absorption coefficients using either theoretical technique; however, it is useful to compare such estimates to those derived from measurement of individual component absorption. The absorption at 441 nm increased from $0.015\ m^{-1}$ near the surface to $0.045\ m^{-1}$ near the fluorescence maximum. At 520 nm, the total range of a was 0.040 to $0.044\ m^{-1}$. Because the diffuse attenuation coefficients were used to calculate the irradiances between the holds, the three-parameter model and the Preisendorfer/Mobley model yielded similar absorption coefficients at four of the five sampling depths (Table 1).

Like Station 8, $\underline{a}$ from the component analysis was much higher than that predicted from apparent optical properties. The differences in $\underline{a}$ were greater for 441 nm than for 520 nm (Table 1) and were high near the surface and at the fluorescence maxima. Only at 100 m for 441 nm, as the particle concentration was declining, was the sum of component absorption less than that derived from apparent optical properties. Since dissolved substances were low at Station 11, the disparity in the absorbances could not be attributed only to difficulty in determining dissolved substance absorption. Even discounting dissolved substance absorption, the sum of particulate and "pure water" absorption still exceeded that derived from the Preisendorfer/Mobley inverse technique. For example, a(520) derived from the theoretical model was about 10% below that of "pure water". Either the model was not accurately predicting absorption, or absorption attributed to pure water was high, or some internal radiance source, such as Raman scattering[15] was influencing the absorption derived from apparent optical properties (the theoretical models).

4.6. Errors in calculation of absorption

The differences between absorption values at 441 nm derived from the theoretical models and absorption calculated as the sum of the components are indicative of errors due to overestimation of absorption by dissolved and suspended material. The determination of a_y is intrinsically difficult and some error is likely. In addition, overestimation of particulate absorption may arise due to uncertainty in the path correction necessary for the Mitchell and Kiefer technique. Measurements from stations with no detectable dissolved

substance component along with ancillary measurements of particulate absorption using opal glass cuvettes have suggested the path length factor may have been underestimated by up to 40%. This would lead to an underestimate of particulate absorption.

Absorption values derived from the theoretical models are subject to uncertainties arising from internal radiance sources such as natural pigment fluorescence, fluorescence of dissolved substances, and Raman scattering, and factors influencing in situ irradiance measurements such as wave focusing and ship contamination. The processing methodology removed much of the uncertainty in irradiances. Stavn and Weidemann[15] have shown that Raman scattering can be a very important factor in explaining the disparity that can arise between absorption values derived from theoretical models and summing components of absorption.

4.7. Particle Characterization

Measurements of individual particle characteristics were made to develop a data set of relevant parameters from which scattering and backscattering coefficients could be estimated and compared to the theoretical estimates of backscatter derived from the Preisendorfer/Mobley model. The results of the beam transmissometry and fluorometry, two accepted in situ methods for estimating total suspended particle concentration and phytoplankton concentrations respectively, have already been described. The "Coulter counter", or more properly the resistive pulse technique is an accepted method for estimating particle concentration and size (volume) distributions. "SAX"[16] (Scanning electron microscopy with Automated image analysis and X-ray spectroscopy) is an automated method whose applicability to particle characterization is being tested. SAX estimates particle concentration and size (projected area) distribution, and additionally gives the elemental composition for each particle, from which we can deduce a refractive index. For comparison to the resistive pulse data, particle volumes were estimated from the SAX data by calculating the diameter of a circle with an area equivalent to the measured particle and then finding the volume of an equivalent sphere. Only the data from Station 11 will be discussed. Because the irradiance values were too low to reliably estimate backscatter below 100 m, only the top three water sample depths (10, 30, and 75 m) were analyzed for particle characterization.

The resistive pulse counts of the total particles in the size range of 1 to 100 um m^{-3} of seawater are about an order of magnitude higher than the SAX results, and the depth profiles of particle counts also differ between the two techniques (Figure 3). The discrepancy probably lies in the lower portion of the size range. Particle concentrations increase logarithmically with decreasing size in the ocean[17], and any differences in the way the two techniques measure the smallest particles will tend to magnify the differences in their total counts.

When the particle numbers are converted to particle volume, the two techniques continue to show differences. The resistive pulse technique detected particles as large as 128 um at all three depths, whereas the SAX technique detected particles no larger than 40 um. This is due to the fact that the seawater volume sampled, 300 ml, contained insufficient numbers of large particles; however, the trend of the differences between the size distributions are clear: the resistive pulse data reveal a relatively flat distribution typical of oligotrophic waters[17]; the SAX data show a shift to fewer and larger particles (Figure 5).

The added dimension of elemental analysis with SAX allows some categorization of the particle population (Figure 6). Of the total particle populations at the three depths, organic particles were the majority: 52, 44, and 56% of the particles at 10, 30, and 75 m respectively. The next most numerous category was ">95% silicon", i.e. diatoms and pieces of diatom frustules: 16, 27, and 30% of the population at each depth. There was a small but persistent population of silicate particles at 8, 8, and 4% respectively. Particles with >95% calcium made up a small fraction of the population at 4, 2, and 1%, and barite was found in trace amounts at all depths. As seen in Figure 6, organic particles tend to dominate the size distribution at all depths. At 10 m silicates are more significant than >95% Si particles in particles larger than 10 um. At 30 m and 75 m, organic and >95% Si distributions are about the same up to a diameter of about 10 um. There is a peak in the >95% Si distribution about 16 um diameter at both depths, and organic particles apparently became larger with depth, peaking about 20 um diameter at 30 m and about 30 um diameter at 75 m.

4.8. Comparison of particle data to backscatter estimates

Qualitative estimates of backscatter based on particle characterizations differ depending on which measure is used. The beam transmissometry data suggests that backscatter should remain fairly constant from the surface to 75 m, while the in situ fluorometry suggests that backscatter might increase slightly around 75 m due to increased

numbers of phytoplankton. Based on the concentration of particles detected by the resistive pulse technique, backscatter should show a peak around 30 m, but, based on the size distributions, there should be little change in backscatter with depth. In contrast, the particle concentration detected by SAX suggests that backscatter should decrease with depth; however, the size and composition data from the SAX analysis suggests that backscatter should increase with depth.

Backscatter estimated from optical measurements using the Preisendorfer/ Mobley model shows an increase to a maximum near 75 m for 441 nm, while backscatter at 520 nm remained fairly constant with depth. The relationships among the various characterizations of suspended particles and the estimates of backscatter derived from the model are not clear at this point due to limitations that are inherent to the measurements and the model. On the one hand, the various results of particle analyses reflect different aspects of the population are being measured; on the other hand, each technique has its own intrinsic errors. For its part, the Preisendorfer/Mobley estimates of backscatter at Station 11 suffer from the same limitation that was seen in the absorbance estimates, namely that the model was not intended for use with only a few widely spaced measurement depths such as the 5 sampling depths spaced by nearly 30 m at this station. In addition, backscatter estimates can be subject to large uncertainties brought about by in situ radiance sources such as Raman scattering and natural fluorescence.

5. CONCLUSIONS

1. Models of Stavn and Preisendorfer/Mobley yielded absorption coefficients that were very similar if the distribution factor was calculated in the Preisendorfer/ Mobley model.

2. At 441 and 520 nm the sum of absorption due to molecular water, dissolved substances, and particulates was higher than absorption values derived from theoretical models.

3. Near the surface, the values of absorption derived from the theoretical models approached absorption coefficients ascribed to molecular water.

4. Preliminary attempts to intercompare particle characteristics and backscatter estimates derived from Preisendorfer/Mobley model have been largely unsuccessful. Increases in backscatter at 441 nm were coincident with fluorescence maxima and increases in organic and siliceous particle size, but backscatter at 520 nm showed very little structure.

5. Internal radiances sources should be investigated as a possible source of error in the theoretical models, and with its inclusion differences in absorbances by the various techniques may diminish.

6. ACKNOWLEDGEMENTS

A. Weidemann wishes to thank the National Research Council which supports his work at NORDA through a Post-Doctoral fellowship.

7. REFERENCES

1. R.W. Preisendorfer, Hydrological Optics, U.S. Dept. of Commerce, NOAA-ERL, Washington, D.C. (1976).
2. R.H. Stavn, "Light attenuation in natural waters: Gershun's law, Lambert-Beer law, and the mean light path," Appl. Opt. 20(4), 2326-2327 (1981).
3. R.H. Stavn, F.R. Schiebe, and C.L. Gallegos, "Optical controls on the radiant energy dynamics of the air/water interface: the average cosine and the absorption coefficient," in Ocean Optics VII, M. Blizard ed., Proc. SPIE 489, 62-67 (1984).
4. R.H. Stavn, "The three-parameter model of the submarine light field: radiant energy absorption and trapping in nepheloid layers recalculated," J. of Geophysical Res. 92(2), 1934-1936 (1987).
5. R.W. Preisendorfer and C.D. Mobley, "Direct and inverse models in hydrologic optics," Limnol. Oceanogr. 29(5), 903-929 (1984).
6. O.V. Kopelevich and V.I. Burenkov, "Relation between the spectral values of the light absorption coefficients of sea water, phytoplanktonic pigments, and the yellow substance," Okeanologiya 17(3), 278-282 (1977).
7. A. Morel and L. Prieur, "Analysis of variations in ocean color," Limnol. Oceanogr. 22(4), 709-722 (1977).
8. R.H. Stavn, "Lambert-Beer law in ocean waters: optical properties of water and of dissolved/suspended material, optical energy budgets," Appl. Opt. 27(2), 222-231 (1988).
9. B.G. Mitchell and D.A. Kiefer, "Determination of absorption and fluorescence excitation spectra for phytoplankton," in Marine phytoplankton and productivity, O. Holm-Hansen, L. Bolis, and R. Gilles ed., pp. 1-13, Springer-Verlag (1984).
10. D.M. Lavoie, "Shape and composition of oceanic particles using an automated SEM/X-ray system," Abstract in Ocean Sciences Proc. (1988).

11. R.C. Smith, K.S. Baker, "The analysis of ocean optical data," in Ocean Optics VII, M. Blizard ed., Proc. SPIE 489, 119-126 (1984).
12. R.C. Smith and K.S. Baker, "Optical properties of the clearest natural waters (200-800 NM)," Appl. Opt. 20(2), 177-184 (1981).
13. A. Bricaud, A. Morel, and L. Prieur, "Absorption by dissolved organic matter of the sea (yellow substance) in the UV and visible domains," Limnol. Oceanogr. 26(1), 43-53 (1981).
14. O.V. Kopelevich, "The yellow substance in the ocean, according to optical data," Okeanologiya 22(2), 152-155 (1982).
15. R.H. Stavn and A.D. Weidemann, "Raman scattering effects in ocean optics," in Ocean Optics IX, M. Blizard ed., Proc. SPIE 925, (1988).
16. D.L. Johnson, "Automated scanning electron microscopic characterization of particulate inclusions in biological tissues," in Scanning Electron Microscopy, Vol III, O. Johari and I. Corvin ed., 1211-1228 (1983).
17. Sheldon, A. Prakash, and W.H. Sutcliffe Jr., "The size distribution of particles in the ocean," Limnol. Oceanogr. 17(3), 327-340 (1972).

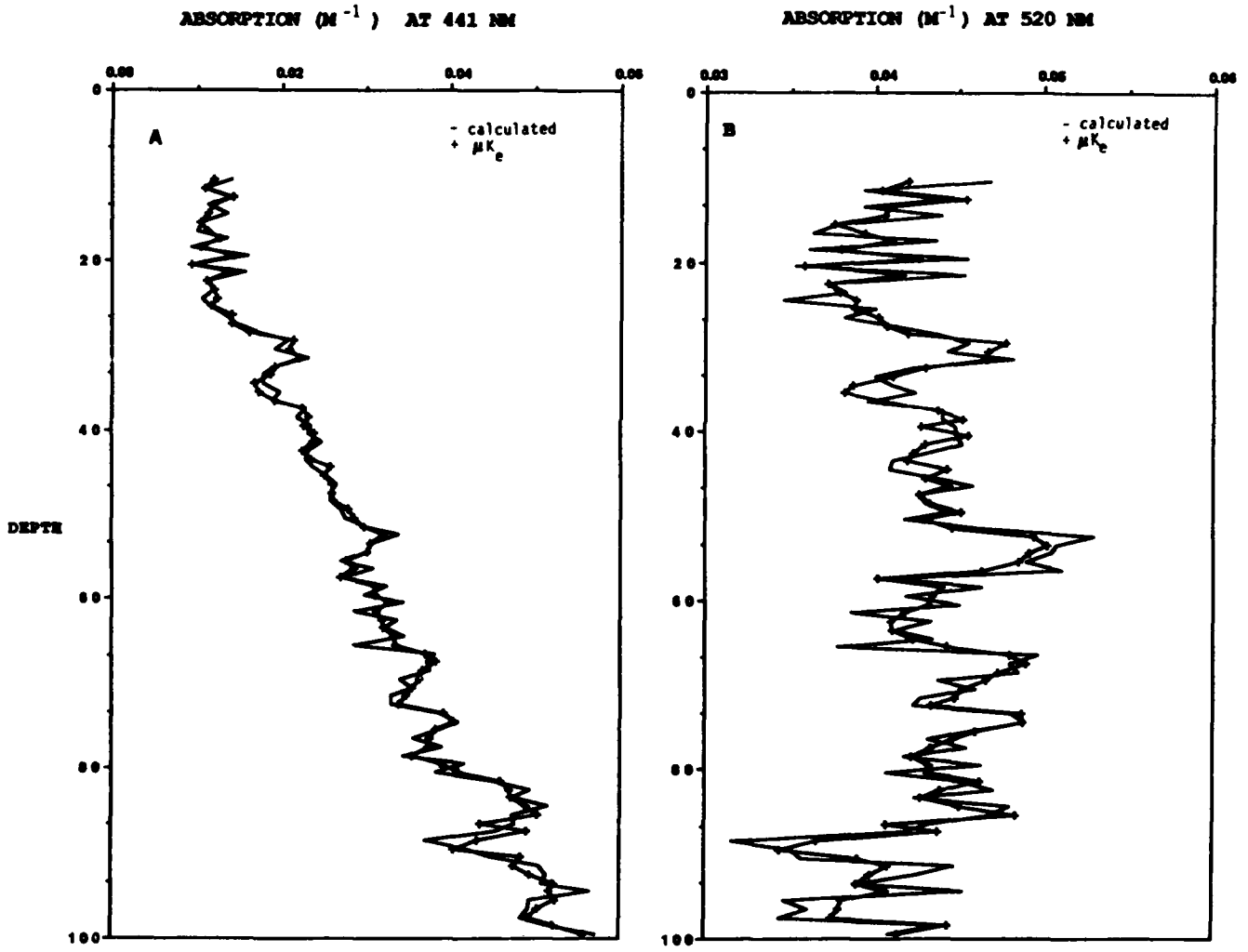

Figure 1. Absorption coefficients at 441 nm (Figure 1A) and 520 nm (Figure 1B) derived using the Preisendorfer/Mobley model with calculated average cosines (-calculated) and the three-parameter model of Stavn (+ uK$_e$).

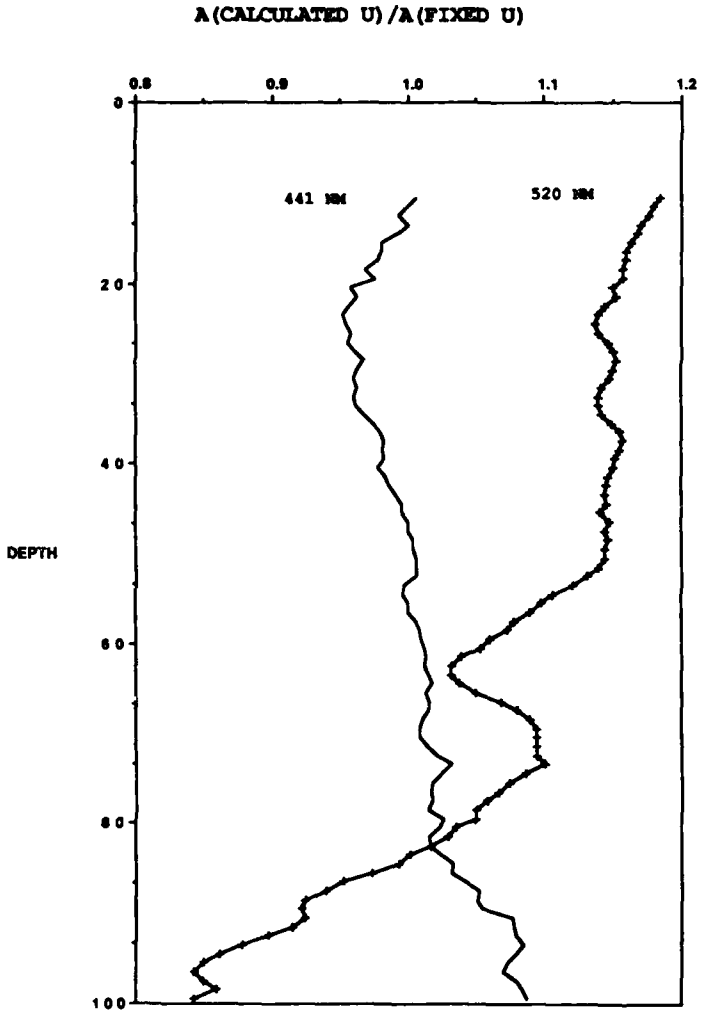

Figure 2. Ratio of absorption coefficient derived from Preisendorfer/Mobley using calculated distribution factors (reciprocal of average cosine) and absorption coefficient derived employing fixed values for distribution factors (1.33 and 2.67 for down- and upwelling respectively) at wavelengths of 441 nm and 520 nm.

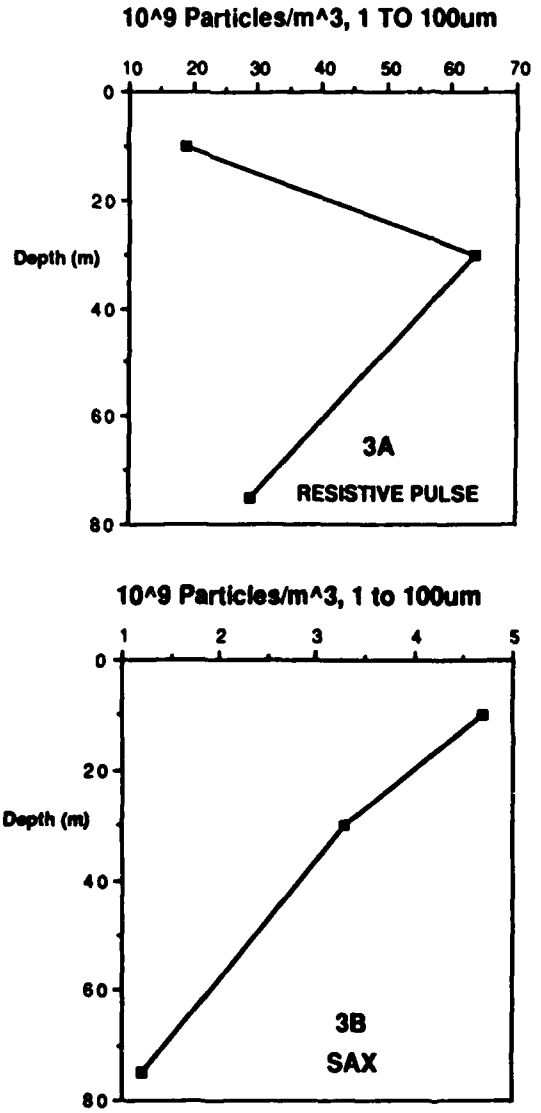

Figure 3. EN 166, Station 11 depth profiles of total particles in the size range of 1 to 100 um. A: by Resistive Pulse ("Coulter Counts"); B: by SAX

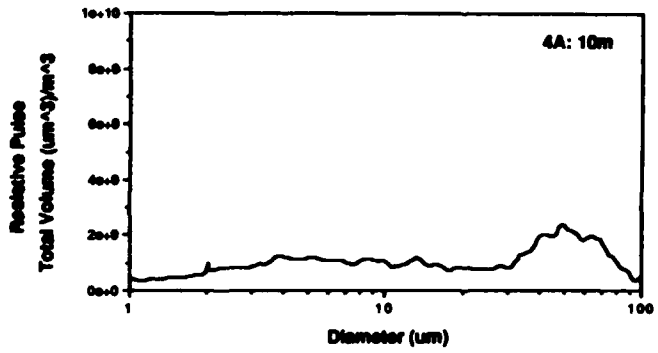

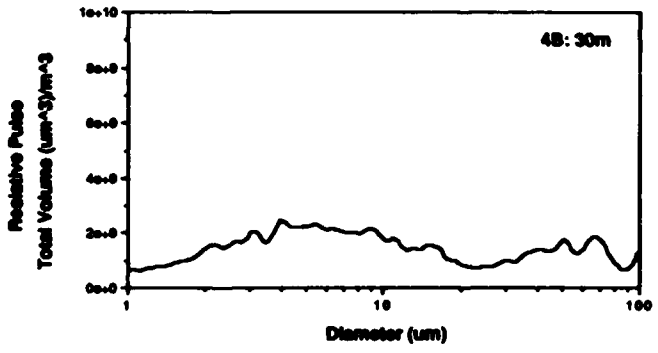

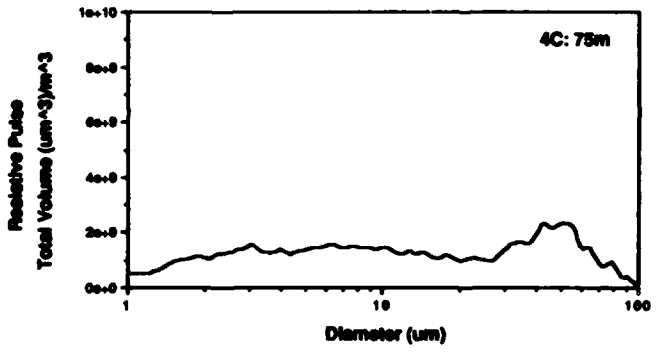

Figure 4. Size distribution of particles by Resistive Pulse for each of the three depths sampled. "Diameter" is the diameter of a sphere with a volume equivalent to the measured particle volume; "Total Volume" is the individual particle volume for a given particle diameter times the total number of particles in that size class per m^3 of Seawater (equivalent to PPB by volume).

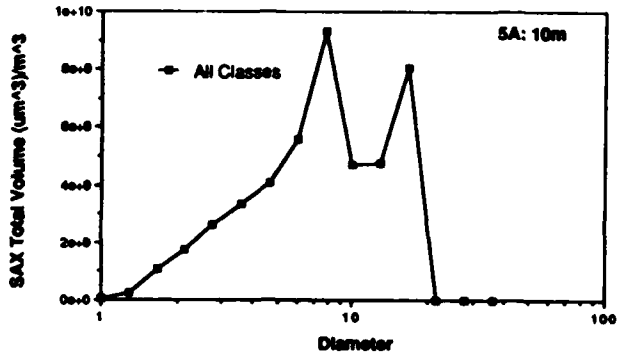

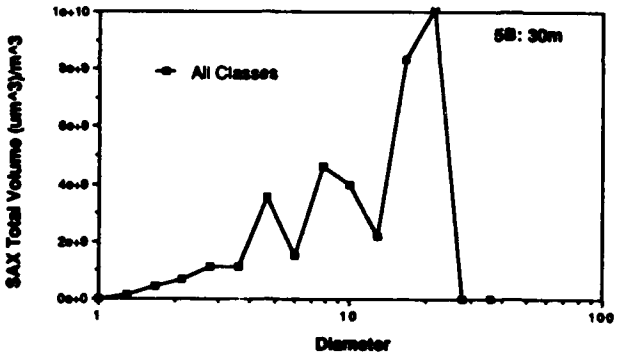

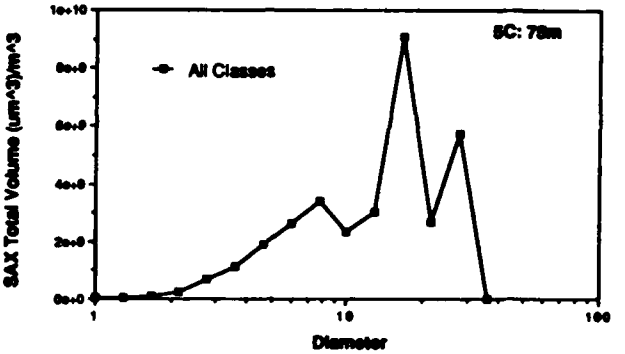

Figure 5. Size distribution of particles of all chemical classes by SAX for each of the three depths sampled. "Diameter" is the diameter of a sphere with a projected area equivalent to the area of the particle measured. "Volume" as in Figure 4.

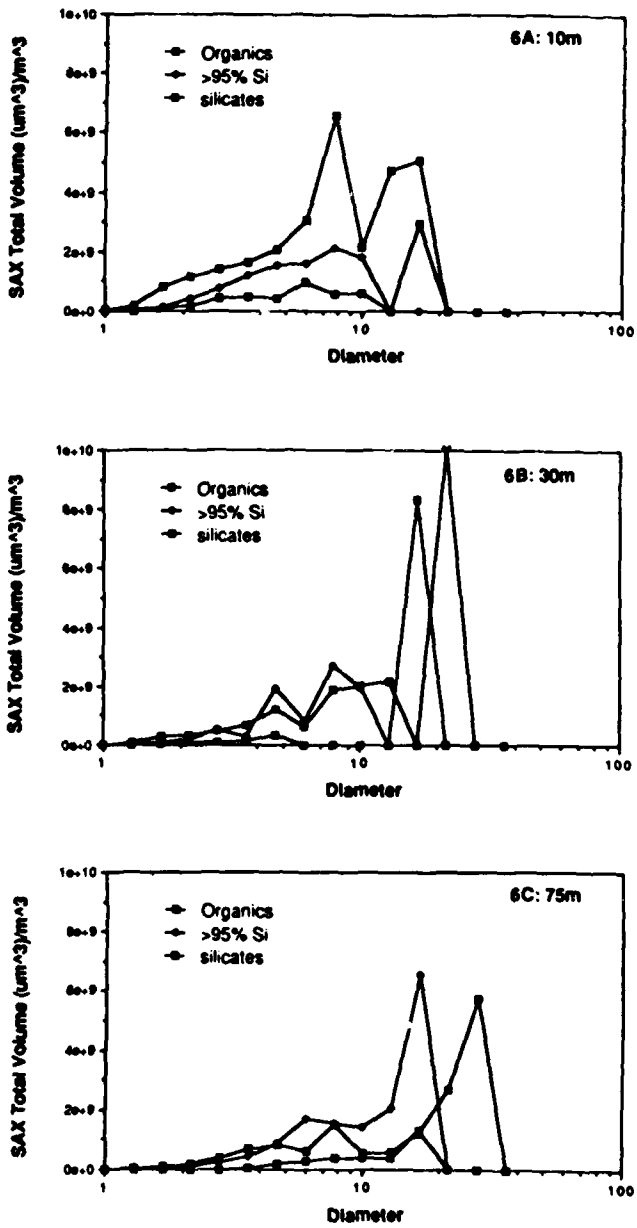

Figure 6. Size distribution of particles in the three major chemical classes. "Diameter" and "Volume" as in Figure 5.